Research Article | Vol. 9, No. 5 / 1 May 2019 / Optical Materials Express 2076
Optical Materials EXPRESS

Laser spectroscopic characterization of negatively charged nitrogen-vacancy (NV^-) centers in diamond

SHOVA D. SUBEDI,[1,*] VLADIMIR V. FEDOROV,[1] JEREMY PEPPERS,[1] DMITRY V. MARTYSHKIN,[1] SERGEY B. MIROV,[1] LINBO SHAO,[2] AND MARKO LONCAR[2]

[1]*Department of Physics, University of Alabama at Birmingham, CH 310, 1300 University Blvd., Birmingham, AL 35294, USA*
[2]*Harvard School of Engineering and Applied Sciences, Cambridge, MA 02138, USA*
[*]*shova1@uab.edu*

Abstract: We report on the spectroscopic and laser characterization of negatively charged nitrogen-vacancy (NV^-) centers in diamond. Spectroscopic properties such as absorption and emission spectra as well as kinetics were studied, and parameters such as cross-sections and lifetimes were estimated. A vibronic band of NV^0 with zero phonon line (ZPL) at 575 nm was detected under 532 nm pulsed excitation due to the photoionization of NV^-. Transmission of 532 nm pump pulses saturate around ~10%, which is much smaller than the theoretical level. $\Delta k/k_0$ kinetics revealed slow recovery of NV^- centers after photoionization under 532 nm pumping, which involved different relaxation channels depending on the probe beam wavelengths. Localization of the electrons in the metastable state of NV^0 centers resulted in higher saturated transmission of 632 nm pump.

1. Introduction

Diamond crystals with impurity perturbed color centers are promising media for lasing over a wide range of the optical spectrum [1–3]. Diamond Raman lasers with very high power and excellent beam qualities have already been reported with very high efficiencies which are needed to meet growing technological demands in applications as diverse as material processing, environmental and remote sensing, and optical communication [4,5]. Additionally, the wide optical transparency range and robust mechanical, thermal, and optical properties of diamond render it an attractive host for color center lasers [6]. Among the numerous color centers in diamond, nitrogen-vacancy (NV) centers, both neutral (NV^0) (with zero phonon line (ZPL) at 575 nm) and negatively charged NV^- (with ZPL at 637 nm) are the most widely studied [7]. The NV center has been extensively investigated due to its stable photoluminescence (PL) and optically measurable and controllable spin states making it an exciting candidate for magnetic sensing, quantum computing, information processing, ultrasensitive nanoscale magnetic field sensing and nanoscale imaging magnetometry [8–14]. Moreover, because of the high gain coefficient, large emission and absorption cross-sections, high quantum efficiency and thermal stability, NV^- color centers can be a promising candidate for lasing in the red to near-infrared region of the optical spectrum.

Each NV center consists of a substitutional nitrogen atom and adjacent lattice vacancy. It has trigonal C_{3v} symmetry with the substitutional nitrogen-lattice vacancy pair oriented along [111] direction [11]. The ground and excited states are spin triplets (S = 1) with principle zero-phonon line (ZPL) at 637 nm (1.945 eV) associated with the radiative transition $^3E \rightarrow {}^3A_2$ [15,16] which is shown as a red wavy line in Fig. 1.

#357791 https://doi.org/10.1364/OME.9.002076
Journal © 2019 Received 16 Jan 2019; revised 18 Mar 2019; accepted 18 Mar 2019; published 5 Apr 2019

Optical Materials EXPRESS

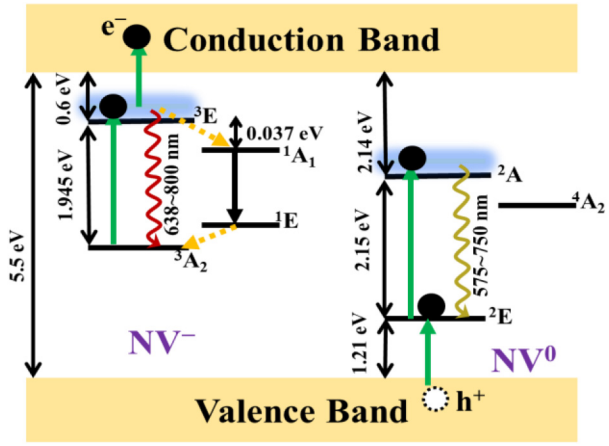

Fig. 1. Relative position of energy levels of NV^- and NV^0 centers in the band gap of diamond (indicated by double-sided arrow lines). Absorption and decay mechanism of NV^- and NV^0 energy levels showing two-step photoionization along with the possible transitions (shown by single-sided arrow lines).

The vibronic transition $^3E \rightarrow {}^3A_2$ in NV^- can be a channel for laser action [1,17]. However, the excited state energy level of NV^- is ~0.6 eV below the conduction band (CB) as shown in Fig. 1. Because of this proximity, with the absorption of second photon the excited electron can be promoted to the CB, instead of decaying back to ground state (radiatively or non-radiatively), thereby photoionizing NV^- centers to NV^0 centers in ground state and leaving a free electron in the CB. During the reverse process, NV^0 absorbs one photon to bring the electron to the excited state, and a second photon brings an electron from the valence band (VB) to the ground state of NV^0, ionizing it to NV^- and leaving a hole in the VB [14]. There is a possibility of photoionization (PI) or ESA in NV^- centers, which may mitigate lasing action of the center [15]. However, there is a recent publication on detection of stimulated emission from NV^- centers in diamond in which the authors observed both spectrally and time-resolved spontaneous emission reduction of NV^- centers under probe laser pulse at wavelengths in the phonon side band (PSB) and interpreted that as a result of stimulated emission in the PSB [13]. However, the reported results are based on indirect measurements and the possibility of direct measurement of optical gain and lasing using NV^- centers is still elusive [13]. In this paper, we performed absorption saturation and pump-probe experiments using a diamond sample with NV^- color centers to clarify the suitability of diamond with NV^- centers for lasing.

2. Experimental results and discussion

2.1. Spectroscopic characterization

The employed sample of size $0.29 \times 3 \times 3$ mm^3 was bulk diamond with a deep purplish pink coloration that was polished on both 3×3 mm^2 facets. The sample was CVD grown by Element Six (UK) Ltd with 200-300 ppm of initial nitrogen concentration. Absorption spectra were measured at room temperature using Shimadzu UV-VIS-NIR-3101PC spectrophotometer. Room temperature absorption measurements were taken with 2 nm spectral resolution at a slow scanning speed of 100 nm/min. Figure 2(a) shows the room temperature absorption spectrum of the sample. An absorption band of pure CVD diamond near the band gap was taken as a baseline and subtracted from the measured absorption spectrum [18]. In Fig. 2(a), an absorption band spanning 500-660 nm with a peak at ~576 nm is due to NV^- centers. Inset graph, Fig. 2(b),

Optical Materials EXPRESS

shows transmission spectrum of the sample without correction for Fresnel reflection. The absorption coefficient is $k \sim 127$ cm^{-1} near the maximum of NV$^-$ absorption. Due to very high concentration of nitrogen, another absorption band with a peak at around 380 nm is also evident. This absorption is due to N3 centers (a vacancy surrounded by three substitutional nitrogen atoms) and the absorption coefficient near the peak of this band was measured to be $k \sim 112$ cm^{-1} [3].

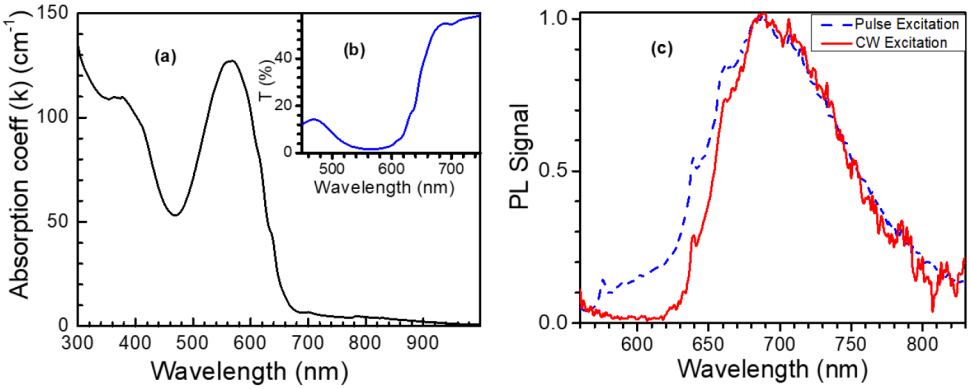

Fig. 2. (a). Absorption spectrum of CVD grown diamond sample. (b) Inset graph shows measured transmission spectrum of the sample without correction for Fresnel reflection (c). The emission spectra measured under CW (red solid curve) and pulsed (blue dashed curve) 532 nm excitation. Under pulsed excitation some of NV$^-$ centers are photoionized to NV^0.

The PL spectra were measured using Acton Research Spectra-Pro 750 monochromator and photomultiplier tube R5108 from Hamamatsu at room temperature. The second harmonic (532 nm) of Spectra-Physics Quanta-Ray Nd:YAG Q-switched pulsed laser operating at 10 Hz repetition rate and a diode pumped Nd:YAG 532 nm CW laser were used as the excitation sources. The measured PL spectra were calibrated with respect to sensitivity of the used spectrometer-detector combination using Oriel standard calibration lamp (model# 63358) and normalized to 1. The normalized fluorescence spectra of the sample with NV$^-$ center ZPL at 638 nm and a wide phonon assisted side band with a maximum at ~700 nm under 532 nm CW excitation (red solid curve) and pulsed excitation (blue dashed curve) are shown in Fig. 2(c). Under pulsed excitation, the intensity of ZPL of NV$^-$ decreases while ZPL of NV^0 at 575 nm starts to appear. This is due to PI of NV$^-$ to NV^0 and is accompanied by an increase of PL signal in the range of 575-630 nm due to the phonon assisted side band of NV^0 centers. The strength of ZPL of NV^0 centers and PSB increases with the increase in the pulse pump power. We measured the emission spectra for pump powers ranging from 2 mW to 50 mW. The measurements had shown the enhancement of ZPL of NV^0 centers and PSB with the increase in the pulse pump power. Our results are in agreement with the results published in N. Aslam et al (2013) and L. Hacquebard et al (2018), where authors reported the increase of ionization and recombination rates with the increase of pump power [15,19].

The kinetics of the PL signal from the sample was measured at different wavelengths using 532 nm pulsed excitation with a pulse duration (10 ns) shorter than the excited state lifetime. Figure 3 shows these decay profiles. The decay lifetimes measured at 576 nm (ZPL of NV^0 centers), 638 nm (ZPL of NV$^-$ centers), 700 nm (near the maximum of emission band) and 830 nm (near the tail of emission band) are 18 ns, 15 ns, 12 ns, and 12 ns, respectively. The decay lifetime of 18 ns near 576 nm is close to the reported lifetime of ^{2}A$\rightarrow^2$E transition of NV^0 center [20]. PL decay lifetime of NV$^-$ corresponding to the transition ^{3}E$\rightarrow^3$A$_2$ at room temperature was estimated to be 12 ns which is close to the reported lifetime 11.6 ns of NV$^-$ centers in the

Optical Materials EXPRESS

literatures [13,21]. These results further support ionization of NV^- centers under pulsed 532 nm excitation.

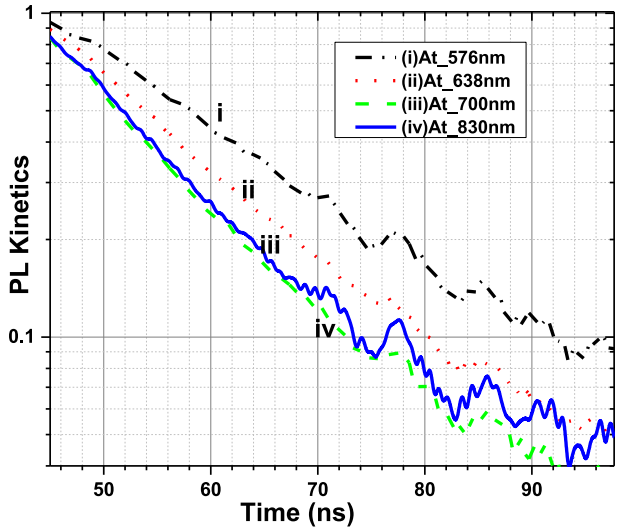

Fig. 3. PL kinetics of NV centers in diamond under 532 nm pulsed excitation (i) at 576 nm (near the ZPL of NV^0 centers), (ii) at 638 nm (near the ZPL of NV^- centers), (iii) at 700 nm (near the peak of emission band), (iv) at 830 nm (near the tail of PL spectrum).

The measured emission spectrum and kinetics were further utilized to estimate the parameters associated with the $^3E \rightarrow {}^3A_2$ transition to allow the calculation of emission cross-section using the method in Ref. [22] adapted for Gaussian shapes:

$$\sigma_{em}(\nu_{0,em}) = \frac{c^2 A_{21}}{8\pi n^2 \nu_{0,em}^2} g_{em}(\nu_{0,em}) \tag{1}$$

$$\sigma_{ab}(\nu_{0,ab}) = \frac{g_2}{g_1} \frac{c^2 A_{21}}{8\pi n^2 \nu_{0,ab}^2} g_{ab}(\nu_{0,ab}) \tag{2}$$

In Eqs. (1) and (2), $g_{em}(\nu_{0,em})$ and $g_{abs}(\nu_{0,abs})$ are the form factors of emission and absorption bands, respectively, which are $\sqrt{4ln2/\pi}/\Delta\nu$ at the central frequencies for a Gaussian distribution, where $\Delta\nu$ is full width at the half maximum and A_{21} is Einstein's coefficient of spontaneous emission. As the quantum yield of NV^- centers in bulk diamond is close to unity ($\phi \approx 1$) [23], we can use the decay lifetime $\tau = 12$ ns obtained from PL kinetics to determine A_{21}. Moreover, $n = 2.4$ is the refractive index of diamond and $g_1 = 1$ and $g_2 = 2$ are degeneracies of the ground and excited states, respectively. The estimated value of absorption and emission cross-sections are 2.8×10^{-17} cm^2 and 4.3×10^{-17} cm^2 at the maximum of absorption and emission bands, correspondingly. We further calculated the absorption cross-section at the pump wavelength (532 nm) to be 2.4×10^{-17} cm^2 using the estimated value of absorption cross-section near the maximum of absorption band and measured absorption spectrum (Fig. 2(a)). Our result is within the error-bar with the cross section ($(3.1 \pm 0.8) \times 10^{-17}$ cm^2) published in Ref. [24]. The stimulated emission cross-section at the maximum is slightly larger than the reported value ($(3.6 \pm 0.1) \times 10^{-17}$ cm^2) in Ref. [25], where it was calculated using Füchtbauer-Ladenburg equation and used 13 ns as the radiative lifetime. The one reported in Ref. [26] is about 7 times higher than our estimated value. However, different fabrication procedure and different combination of the color centers could have some influence on inhomogeneous broadening and

Optical Materials EXPRESS

maximum emission and absorption cross sections. Using the value of absorption cross-section at the peak and absorption coefficient from Fig. 2(a), the concentration of NV^- center is found to be ~25 ppm (4.5×10^{18} cm^{-3}).

2.2. Laser characterization under 532 nm pumping

The PI of neutral (NV^0) and negative (NV^-) charge states as well as possible ESA processes are the major mechanisms impeding the possibility of lasing. Hence, it is very critical to understand the dynamics of ESA and PI. For this purpose, we performed absorption saturation experiments based on measurement of the transmission of incident radiation through the sample for different incident energy fluences. In general, fractional absorption of incident light decreases with the increase of pump intensity and the system should become more transparent to the incident light. At sufficiently high intensity (typically above saturation intensity), the transmission will saturate and becomes relatively constant despite any further increase in intensity. Here, we used a 532 nm pump beam with a beam diameter of 1.6 mm and repetition rate 10 Hz. A combination of a half wave plate and a Glan prism was used to vary the incident fluence. Transmission of pump energy fluence is measured by taking the ratio of transmitted pump fluence through the sample and the incident pump fluence. The red dotted curve (ii) in Fig. 4 depicts transmission measured at different pump energy fluence. As pump energy increases, transmission increases from its initial value of $T_0 \approx 3\%$ and saturates at $T_s \approx 10\%$ for higher energy fluence. Transmission is less sensitive at higher pump fluence (>100 mJ/cm^2). We compare our measured transmission with that predicted by the Frantz-Nodvik equation given in Eq. (3) [27] and represented by a blue dashed curve (i). $E_s(\nu) = h\nu/\sigma_{abs}(\nu)$ is saturation fluence calculated at pump wavelength 532 nm, whose value is 15.5 mJ/cm^2, where $\sigma_{abs} \approx 2.4\times10^{-17}$ cm^2 is the absorption cross-section at 532 nm measured using the absorption spectrum, and $T_0 = 3\%$ is the initial transmission extracted from the transmission spectrum measured by spectrophotometer.

$$T = \frac{E_s}{E_{in}} ln\left[1 + \left(e^{\frac{E_{in}}{E_s}} - 1\right) T_0\right] \tag{3}$$

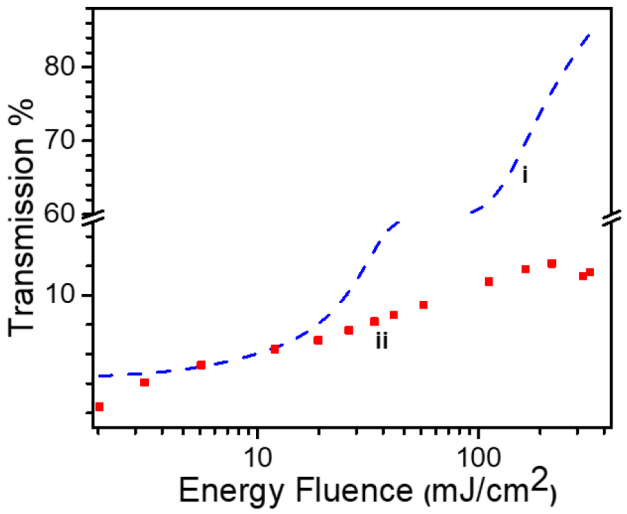

Fig. 4. Variation of a 532 nm pump beam transmission through the sample as a function of a pump energy fluence (i) calculated using Frantz-Nodvik equation (blue dashed line) and (ii) measured (red dotted curve).

It can be seen from Fig. 4 that as pump energy flux increases, the measured transmission strongly deviates from the values calculated using the Frantz-Nodvik equation. This indicates

Optical Materials EXPRESS

that there exists a strong absorption of pump photon even after the bleaching of NV^- ground state. One possible mechanism could be induced long-term bleaching of the centers. However, transmission spectra measured before and immediately after long 532 nm pulsed illumination did not show any changes. Another possible mechanism for such a small transmission is PI and/or ESA. The latter mechanism is further supported by photoionization of NV^- and formation of NV^0 centers as illustrated in Fig. 2(c) and Fig. 3.

We designed several nonselective Fabry-Perot cavities that would minimize loss and increase positive feedback in order to obtain lasing under Nd: YAG 532 nm pulsed excitation. One of these Fabry-Perot cavities was formed by using HR (at 600-800 nm) mirror and the Fresnel reflection from the output facet of the sample and had a length of ~1 cm. The sample was pumped with up to 560 mJ/cm^2 at 532 nm, which is about 35 times the saturation energy fluence (15.5 mJ/cm^2). We did not observe stimulated emission or lasing under 532 nm pumping.

2.3. Pump-probe experiment at different probe wavelengths

To study the dynamics of the absorption at possible oscillation wavelengths after excitation, we performed a pump-probe experiment using 532 nm pump pulses and two CW probe beams at 632 nm (HeNe laser) and 670 nm (fiber-pigtailed diode laser). The temporal resolution of the pump-probe experiments was larger than the upper level lifetime of both NV^0 and NV^- centers (~20 ns).

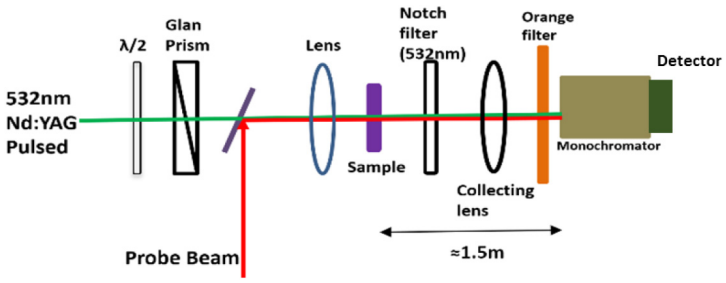

Fig. 5. Schematic diagram of the pump probe experiment.

Figure 5 is a schematic diagram of a setup for the pump probe experiment. The second harmonic of Nd:YAG pulsed pump laser radiation of 60 mW average power with 10 Hz repetition rate along with the CW probe beams of ~5 mW power was utilized. Beam size of the green pulse near sample was about 1.6 mm in diameter which gives ~300 mJ/cm^2/pulse. This is the range of the pump densities where the absorption of the pump saturates (see Fig. 4). Such a high energy density would activate any long-lived kinetics, if any present. A series of filters was used to block the scattered pump beam from the detector. The transmitted signals at probe beam wavelengths were measured by the Spectrapro-300i monochromator along with a PMT detector (PM tube R928 from Hamamatsu in housing PD439 from Acton Research Corporation)) and recorded by an oscilloscope. Figures 6(a) and 6(b) show the decay dynamics of the signal measured at probe wavelengths, where curves 'i' are the signals measured at probe wavelengths using 532 nm pump and probe beams simultaneously incident on the sample. We blocked the pump beam and measured probe signal (curves 'ii') and blocked the probe beams and measured PL signal at probe wavelengths (curves 'iii') as shown in figures below. Measured transmissions in Figs. 6(a) and 6(b) were not corrected for Fresnel reflection which is ~17% at each crystal surface. Steady state transmission of 632 nm and 670 nm, curves 'ii', are consistent with the initial transmission measured using spectrophotometer (see Fig. 2(b)). In the presence of the 532 nm pump pulse, the transmission of 632 nm probe beam increases from initial value ~17% to ~26%. On the other hand, 670 nm probe beam transmission increases from ~50% to ~56% after the pump pulse. A

Optical Materials EXPRESS

spike in Fig. 6(b) curve 'iii', under 532 nm pump alone, is due to the NV^- luminescence signal reaching the detector. The curve 'iii' shows influence of "parasitic photoluminescence signal " on the probe beam, which could be neglected after 20 ns of transmission kinetics.

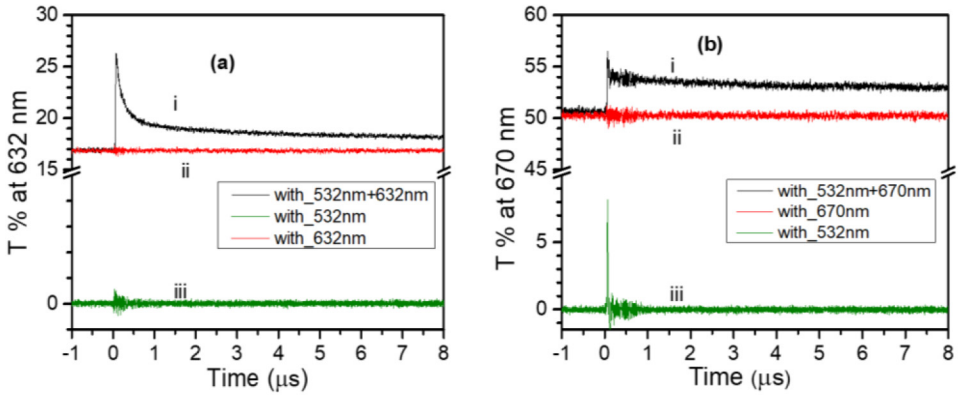

Fig. 6. Signal measured at probe wavelengths (a) 632 nm and (b) 670 nm, respectively, using (i) 532 nm pump beam and probe beam simultaneously, (ii) probe beam only (after blocking the 532 nm pump beam), and (iii) 532 nm pump beam only (after blocking the probe beam) which represents PL signal at the probe wavelength.

The pump-induced change in transmission of the probe beams gives the picture of temporal evolution of population density of the corresponding center. As one can see from Fig. 2(a), the absorption of the probe beam at 632 nm is primarily the result of NV^- centers and could be used to test the dynamic of the NV^- centers concentration. It should be noted that at both wavelengths, we observed an increase of the probe transmissions. This indicates that any induced absorption is smaller than bleaching due to the ionization process. In addition, the kinetics at 632 nm (Fig. 6(a)) reveals a multi-exponential behavior with "fast" decay and "slow" decay channels. On the other hand, there is no relaxation stage kinetic at 670 nm corresponding to "fast" decay (Fig. 6(b)), implying that absorption at 670 nm is induced by another color center. We can see the transmission recovery to the steady state level (curves 'ii' in Figs. 6(a) and 6(b)) between the pulses (100 ms) for both 632 nm and 670 nm kinetics. Centers recover to the initial level which implies no residual absorption or long-term bleaching (>100 ms) for 10 Hz repetition rate.

The temporal recovery of the initial concentration of the ionized centers could be analyzed using $\Delta k/k_0$ plots (see Fig. 7), where Δk is the change of the absorption coefficient and k_0 is the initial absorption coefficient at probe wavelength. If there is only one type of centers present, $\Delta k/k_0$ ratio does not depend on cross-section and $\Delta k/k_0 \sim \Delta n/n_0$ is same for all wavelengths, where $\Delta n/n_0$ represents fractional population inversion. The probe kinetics at 632 nm could be fit by two exponential curves with 250 ns and 12 μs time constants. The fast decay time is close to the reported lifetime of the metastable level of NV^- centers [27]. The slow kinetics could be explained by the capture of the electron after ionization of NV^- centers by a deep trap followed by a slow recovery process. The recovery time of the absorption at 670 nm was calculated to be 24 μs. Kinetics of transmission of different probe beams show that the ionization and bleaching process involves different channels indicated by different recovery times.

2.4. Absorption saturation measurement under 632 nm pumping

In an attempt to mitigate PI processes of NV^- centers, we decided to test a 632 nm pulsed laser pump as our new excitation source. This wavelength should excite NV^- but not NV^0, which could be helpful in mitigating the back-and-forth PI processes. Raman shifted radiation of the second harmonic of Nd:YAG laser from a deuterium cell at 632 nm was used for pumping. The

Optical Materials EXPRESS

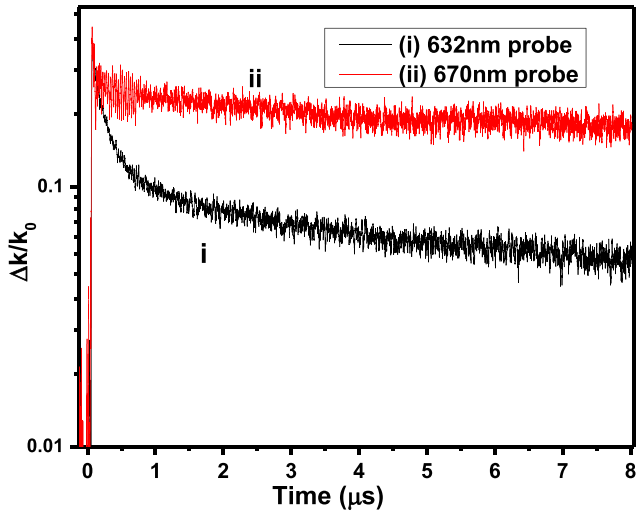

Fig. 7. Comparison of evolution of $\Delta k/k_0$ kinetics under 532 nm pumping at probe wavelengths (i) at 632 nm and (ii) at 670 nm.

pump source had 10 ns pulse duration and operated at 10 Hz repetition rate. We performed an absorption saturation measurement as described in section 2.2 and measured the transmission of the pump at different input intensities of 632 nm pump pulses. The measured transmission corrected for Fresnel reflection level is plotted red dotted curve in Fig. 8. We compared our measured transmission with that predicted by the Frantz-Nodvik equation given in Eq. (3) [28] and represented by a blue dashed curve 'i' in Fig. 8. Saturation fluence is calculated using $E_s(\nu) = h\nu/\sigma_{abs}(\nu)$ at pump wavelength 632 nm, whose value is 30.2 mJ/cm^2, where $\sigma_{abs} \approx 1.1\times10^{-17}$ cm^2 is the absorption cross-section at 632 nm estimated using the absorption spectrum, and $T_0 = 25.7\%$ is the initial transmission extracted from the transmission spectrum measured by spectrophotometer after correction to Fresnel reflection.

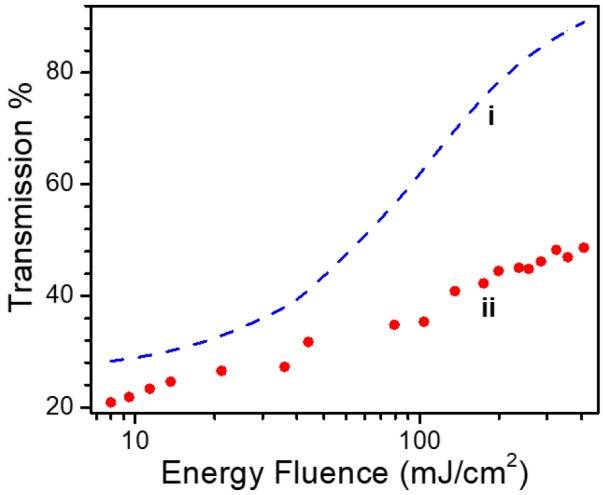

Fig. 8. The dependence of 632 nm pump transmission through the sample as a function of a pump energy fluence (i) calculated using Frantz-Nodvik equation (blue dashed line) and (ii) measured from the experiment (red dotted curve).

Optical Materials EXPRESS

The saturated transmission level under 632 nm was significantly higher than that measured under 532 nm pumping (see Fig. 4). The transmission at 632 nm increased from $T_0 \approx 21\%$ to $T_s \approx 48\%$ for pulses with energy fluence >300 mJ/cm^2. We measured saturation of the absorption at 632 nm pump which was stronger than that under 532 nm excitation. However, the saturated transmission near 400 mJ/cm^2 is still ~2 times smaller than it would be when calculated using Frantz-Nodvik equation. It shows that the PI is still present. Furthermore, to detect any long lived photo-ionization or bleaching of the centers, we measured transmission before and immediately after (within less than a minute) illumination of the sample under 632 nm pump. We irradiated the sample at sufficiently high energy fluence (>3 J/cm^2/pulse), which is near optical damage threshold, for about twenty minutes. Our measurement shows no change in the transmission profile meaning no long-lived residual absorption. However, additional experiments are required to estimate the ratio of excited and ionized color centers.

We designed non-selective Fabry-Perot resonator which with gold-plated concave mirror (R = 5 cm) working as a high reflector and polished facet of the sample as an output coupler (Fresnel reflection ~17%). The length of the cavity was ~3.5 cm. The spectral profile of the NV$^-$ centers emission did not show any notable change up to pump energy density of 0.5 J/cm^2. However, experiment with optimization of the pump energy and cavity designs are still under study and will be reported later.

2.5. Model describing the saturation and pump-probe kinetics

The results from the saturation and pump-probe experiments could be summarized as follows:

- Variation of the transmission values at 532 nm from small pump signal to pulse energy density $E = 350$ mJ/cm^2 was relatively small: from $T_0 = 0.03$ to $T = 0.1$.
- The transmission values at 632 nm from small pump signal to pulse energy density E = 400 mJ/cm^2 was measured to be $T_0 = 0.20$ and $T = 0.48$, respectively.
- There was no excited state absorption at 632 nm and 670 nm probe wavelengths.
- The absence of the laser oscillation under 532 nm excitation indicates low population densities of the NV^0 and NV$^-$ color centers on upper laser levels.

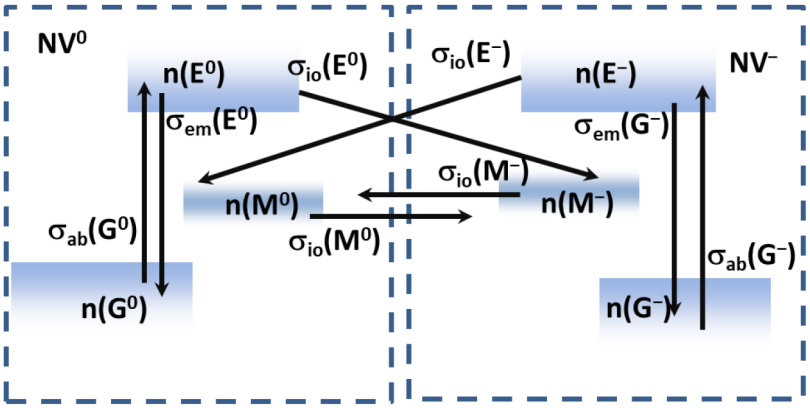

Fig. 9. Illustration of the energy levels of NV^0 and NV$^-$ centers and corresponding population densities and cross-sections used to describe the proposed model of saturation and pump-probe experiments.

Optical Materials EXPRESS

One of the models describing the results from saturation and pump-probe measurements is shown in Fig. 9 above. The proposed model considered both NV^0 and NV^- centers as a three-level system. The rate equations for each level are:

$$\begin{cases} \dot{n}(G^0) = -I_p\sigma_{ab}(G^0)n(G^0) + I_p\sigma_{em}(E^0)n(E^0) \\ \dot{n}(G^-) = -I_p\sigma_{ab}(G^-)n(G^-) + I_p\sigma_{em}(E^-)n(E^-) \\ \dot{n}(E^0) = I_p\sigma_{ab}(G^0)n(G^0) - I_p\sigma_{em}(E^0)n(E^0) - I_p\sigma_{io}(E^0)n(E^0) \\ \dot{n}(E^-) = I_p\sigma_{ab}(G^-)n(G^-) - I_p\sigma_{em}(E^-)n(E^-) - I_p\sigma_{io}(E^-)n(E^-) \\ \dot{n}(M^0) = I_p\sigma_{io}(E^-)n(E^-) - I_p\sigma_{io}(M^0)n(M^0) - I_p\sigma_{io}(M^-)n(M^-) \\ \dot{n}(M^-) = -I_p\sigma_{io}(E^0)n(E^0) + I_p\sigma_{io}(M^0)n(M^0) + I_p\sigma_{io}(M^-)n(M^-) \end{cases} \tag{4}$$

Where, $n(G^0)$, $n(E^0)$, $n(M^0)$ and $n(G^-)$, $n(E^-)$, $n(M^-)$ are population densities at ground state (G), excited state (E) and metastable state (M) of NV^0 and NV^- color centers, correspondingly, where superscript denotes charge state of the center. Similarly, $\sigma_{ab}(G^0)$, $\sigma_{ab}(G^-)$ and $\sigma_{em}(E^0)$, $\sigma_{em}(E^-)$ are absorption and emission cross-section of ground and excited states of NV^0 and NV^- respectively. In the Fig. 9, arrows show all the possible excitation, emission and PI paths for NV^0 and NV^- which we considered in our model. We consider only photo-induced process and disregard relaxation process under excitation. Under high density excitation pulses at times (i.e. $\tau >> 1/I_p\sigma_{io}$) the populations reach saturation levels, all the time derivatives equal to zero. This gives;

$$n(G^0) = n(G^-) = n(E^0) = n(E^-) = 0 \tag{5}$$

$$n(M^-) = n(M^0)[\sigma_{io}(M^0) \Big/ \sigma_{io}(M^-)] \tag{6}$$

$$n(M^0) + n(M^-) = N_{total} \tag{7}$$

In the case when $\sigma_{io}(M^0) \approx \sigma_{io}(M^-) \equiv \sigma_{io}$, the transmission of the excitation beam changes from initial value $T_0 = exp(-\sigma_{ab}(G^-)LN_{total})$ to saturated level $T_s = exp(-\sigma_{io}LN_{total})$.

This model is also in a good agreement with results reported in Ref. [15]. In this paper it was reported that the ratio of the photo-ionization rates for $NV^- \rightarrow NV^0$ process and for $NV^0 \rightarrow NV^-$ processes is ~0.4 at 540 nm excitation wavelength. If we will use this ratio for photoionization processes and change of transmission at 532 nm from $T_0 = 3\%$ to $T_s = 10\%$ from our experiment, we could find the relation between absorption and photoionization cross-sections as $\sigma_{io}(M^-) \approx 0.5\sigma_{ab}(G^-)$ at 532 nm. It is noteworthy that this ratio does not depend on other parameters of the model.

In the case when $\sigma_{io}(M^0) \approx 0$ (i.e. $\sigma_{io}(M^0) << \sigma_{io}(M^-)$), the population $n(M^-) = 0$, and all the centers will be localized at $n(M^0) \approx N_{total}$, where the absorption at pump wavelength is neglectable $\sigma_{io}(M^0) \approx 0$. In this case the transmission of the excitation pulse will increase from the initial value T_0 to 1 for high pump intensity. This case was observed under 632 nm excitation. It is also in agreement with the data reported in [15] where the photo-ionization rates for $NV^- \rightarrow NV^0$ process was significantly bigger than that for $NV^0 \rightarrow NV^-$.

This model also describes recovery dynamic of $\Delta k/k_0$ at 632 nm. As we discussed above, after excitation the ratio of the concentrations at metastable levels using Eq. (6) $n(M^0)/n(M^-)$ which is ~ 0.4 based on data reported in Ref. [15]. The recovery of the absorption to the initial level will consist of decays of the metastable states of NV^0 and NV^- centers. The decay time of the $n(M^-)$ was measured to be $\tau(M^-) = 250$ ns at room temperature [27], while recovery time for $NV^- \rightarrow NV^0$ process was significantly slower (>10 μs) [29]. In this case, $\Delta k/k_0$ should be multi exponential with "fast" decay rate 250 ns and amplitude ratio between "slow" and "fast" kinetics $n(M^0)/n(M^-) \approx 0.4$. As one can estimate from Fig. 7, the amplitude ratio for the fast and slow

Optical Materials EXPRESS

kinetics at 632 nm is approximately 0.4. This indicates strong PI of NV^- and increase of the population to the metastable state of NV^0 centers.

The absences of "fast" kinetics for the pump-probe experiments at 670 nm results probably from the strong influence on absorption from other color centers. As one can see from the Fig. 2(a), there is an overlap between NV^- color centers absorption band with another band with maximum ~700 nm. The analysis of the induced photo effects at this wavelength requires additional study.

3. Conclusions

In conclusion, we have measured absorption and emission spectra of NV^- centers in a CVD grown diamond sample at room temperature and estimated the absorption and emission cross-sections to be 2.8×10^{-17} cm^2 and 4.3×10^{-17} cm^2 at the maximum of absorption and emission bands, respectively, which are in close agreement with reported values documented in the literature. Concentration of NV^- centers in the diamond sample was estimated to be ~25 ppm (4.53×10^{18} cm^{-3}). We observed appearance of ZPL of NV^0 along with a broad PSB under pulsed excitation due to photoionization of NV^- to NV^0. We also estimated the decay lifetime of the excited state of NV^- to be 12 ns from PL kinetics at room temperature. Saturated transmission of 532 nm pump pulse was only ~10% even at energy flux much higher than saturation level and we did not detect any induced long-term bleaching of the centers. In a pump-probe experiment the transmission kinetics at 632 nm reveal a "fast" decay process with recovery time ~250 ns and a "slow" decay process with recovery time ~12 µs. On the other hand, only a "slow" (recovery time 24 µs) decay channel appeared in the kinetics of transmission at 670 nm. This indicates different decay channels involved after photoionization of NV^- centers under green excitation. Centers recover to steady state level between the pulses showing no residual absorption or long-lived bleaching for 10 Hz repetition rate. We did not detect long lived photo-ionization or bleaching of the centers after irradiating under strong 532 nm pump density. Transmission saturates to ~48% under 632 nm pump which was stronger than that under 532 nm pumping. Pumping at 632 nm with sufficiently high intensity leads to the accumulation of electrons in metastable state of NV^0 center resulting in higher saturation of transmission. We setup a resonator using polished face of the sample and gold-plated concave mirror and measured spectral profile at different intensities. We did not measure notable change in full width at half maximum (FWHM) of emission band. That implies population of excited state of NV^- is still small, since we do not see stimulated process or lasing. However, additional experiments are required to estimate the ratio of excited and ionized color centers. The optimization of the pump energy and cavity designs are still under study and will be reported later.

Funding

Defense Advanced Research Projects Agency (DARPA) (0008, 1, 15, W31P4Q).

Acknowledgements

The authors would like to thank Dr. Matthew Markham from Element Six (UK) for providing diamond sample.

References

1. M. A. Prelas and L.-T. S. Lin, "Laser modes in diamond," *Conference paper: Wide Band Gap Electronic Materials, Springer, Dordrecht*, 187–206 (1995).
2. F. Jelezko, C. Tietz, A. Gruber, I. Popa, A. Nizovtsev, and S. Kilin, "Spectroscopy of Single N-V Centers in Diamond," Single Mol. **2**(4), 255–260 (2001).
3. L. G. Deshazer and S. C. Rand, "Visible color-center laser in diamond," Opt. Lett. **10**(10), 481–483 (1985).
4. R. J. Williams, O. Kitzler, Z. Bai, S. Sarang, H. Jasbeer, A. McKay, S. Antipov, A. Sabella, O. Lux, D. J. Spence, and R. P. Mildren, "High Power Diamond Raman Lasers," IEEE J. Sel. Top. Quantum Electron. **24**(5), 1–14 (2018).

Optical Materials EXPRESS

5. K. D. Jamison and H. K. Schmidt, "Doped diamond laser," U.S. Patent 5504767 (1996).
6. R. P. Mildren and A. Sabella, "Highly efficient diamond Raman laser," Opt. Lett. **34**(18), 2811–2813 (2009).
7. A. Zaitsev, *Optical Properties of Diamond* (Springer, 2000).
8. W. L. Yang, Z. Q. Yin, Y. Hu, M. Feng, and J. F. Du, "High-fidelity quantum memory using nitrogen-vacancy center ensemble for hybrid quantum computation," Phys. Rev. A **84**(1), 010301 (2011).
9. C. L. Degen, "Scanning magnetic field microscope with a diamond single-spin sensor," Appl. Phys. Lett. **92**(24), 243111 (2008).
10. G.K. Balasubramanian, I. Y. chan, R. Lolesov, M. Al-Mmoud, J. Tisler, C. Shin, C. Kim, A. Wojcik, P. R. Hemmer, A. Krueger, T. Hanke, A. Leitenstorfer, R. Bratschitsch, F. Jelezko, and J. Wrachtrup, "Nanoscale imaging magnetometry with diamond spins under ambient conditions," Nature **455**(7213), 648–651 (2008).
11. J. Walker, "Optical absorption and luminescence in diamond," Rep. Prog. Phys. **42**(10), 1605–1659 (1979).
12. M. W. Dohetry, N. B. Manson, P. Delaney, F. Jelezko, J. Wrachtrup, and C. L. Hollenberg, "The nitrogen-vacancy color center in diamond," Phys. Rep. **528**(1), 1–45 (2013).
13. J. Jeske, D. W. M. Lau, X. Vidal, L. P. McGuinness, P. Reineck, B. C. Johnson, M. W. Doherty, J. C. McCallum, S. Onoda, F. Jelezko, T. Ohshima, T. Volz, J. H. Cole, B. C. Gibson, and A. D. Greentree, "Stimulated emission from nitrogen vacancy centers in diamond," Nat. Commun. **8**, 14000 (2017).
14. E. Bourgeois, A. Jarmola, P. Siyushev, M. Gulka, J. Hruby, F. Jelezko, D. Budker, and M. Nesladek, "Photoelectric detection of electron spin resonance of nitrogen-vacancy centers in diamond," Nat. Commun. **6**(1), 8577 (2015).
15. N. Aslam, G. Waldherr, P. Neumann, F. Jelezko, and J. Wratchup, "Photoinduced ionization dynamics of the nitrogen vacancy defect in diamond investigated by single-shot charge state detection," New J. Phys. **15**(1), 013064 (2013).
16. L. J. Rogers, M. W. Doherty, M. S. Barson, S. Onoda, T. Ohshima, and N. B. Manson, "Singlet levels of the NV-centers in diamond," New J. Phys. **17**(1), 013048 (2015).
17. O. A. Shenderova and D.M. Gruen, "Ultra-nanocrystalline diamond: Synthesis, Properties and Applications," Elsevier, Oxford, UK (2012).
18. H. C. Lu, Y. C. Peng, M. Y. Lin, S. L. Chou, J. I. Lo, and B. M. Cheng, "Photoluminescence of a CVD Diamond Excited with VUV Light from a Synchrotron," Opt. Photonics J. **3**(6), 25–28 (2013).
19. L. Hacquebard and L. Childress, "Charge-state dynamics during excitation and depletion of the nitrogen-vacancy center in diamond," Phys. Rev. A **97**(6), 063408 (2018).
20. G. Liaugaudas, G. Davies, K. Suhling, R. U. Khan, and D. J. Evans, "Luminescence lifetimes of neutral nitrogen-vacancy centers in synthetic diamond containing nitrogen," J. Phys.: Condens. Matter **24**(43), 435503 (2012).
21. A. T. Collins, M. F. Thomaz, and M. I. B. Jorge, "Luminescence decay time of the 1.945 eV centre in type Ib diamond," J. Phys. C: Solid State Phys. **16**(11), 2177–2181 (1983).
22. C. C. Davis, *Laser and Electro-optics: Fundamental and Engineering* (Cambridge University Press, 2014).
23. A. Gruber, A. Dräbenstedt, C. Tietz, L. Fleury, J. Wrachtrup, and C. von Borczyskowski, "Scanning confocal optical microscopy and magnetic resonance on single defect centers," Science **276**(5321), 2012–2014 (1997).
24. T. L. Wee, Y. K. Tzeng, C. C. Han, H. C. Chang, W. Fann, J. H. Hsu, K. M. Chen, and Y. C. Yu, "Two-photon Excited Fluorescence of Nitrogen-Vacancy Centers in Proton-Irradiated Type Ib Diamond," J. Phys. Chem. A **111**(38), 9379–9386 (2007).
25. E. Fraczek, V. G. Savitski, M. Dale, B. G. Breeze, P. Diggle, M. Markham, A. Bennett, H. Dhillon, M. E. Newton, and A. J. Kemp, "Laser spectroscopy of NV- and NV^0 colour centres in synthetic diamond," Opt. Mater. Express **7**(7), 2571–2585 (2017).
26. V. G. Vins and E. V. Pestryakov, "Color centers in diamond crystals: Their potential use in tunable and femtosecond lasers," Diamond Relat. Mater. **15**(4-8), 569–571 (2006).
27. V. M. Acosta, A. Jarmola, E. Bauch, and D. Budker, "Optical properties of the nitrogen-vacancy singlet levels in diamond," Phys. Rev. B **82**(20), 201202 (2010).
28. W. Koechner, *Solid-State Laser Engineering* (Springer, 1999).
29. N. B. Manson and J. P. Harrison, "Photo-ionization of the nitrogen-vacancy center in diamond," Diamond Relat. Mater. **14**(10), 1705–1710 (2005).